# Electronic Supplementary Material

# Hierarchically mesoporous Ce-Based MOFs with enhanced alkaline phosphatase-like activity for phosphorylated biomarkers sensing

Rui Gao[a], Niru Ye[a], Xiaoxue Kou[a], Yujian Shen[a], Huangsheng Yang[a], Tong Wu[a], Siming Huang[b]*, Guosheng Chen[a]* and Gangfeng Ouyang[a]

[a]MOE Key Laboratory of Bioinorganic and Synthetic Chemistry, School of Chemistry, Sun Yat-sen University, Guangzhou 510275, China

[b]School of Pharmaceutical Sciences, Guangzhou Medical University, Guangzhou 511436, China

## This file including:

**S1. Methods and materials**

**S2. Supplementary Figures**

**S3. Supplementary Tables**

**S4. Supplementary References**

## S1. Methods and materials

**Reagent and materials.**

1,4-dicarboxybenzene (BDC), sodium perchlorate monohydrate ($NaClO_4 \cdot H_2O$), 4-methylumbelliferone phosphate (4-MUP), 4-methylumbelliferone (4-MU), malachite green, uric acid, and NaOH were purchased from Aladdin Chemistry Co., Ltd. (Shanghai, China). Adenosine triphosphate (ATP), cerium ammonium nitrate $(NH_4)_2Ce(NO_3)_6$, and 4-(2-hydroxyethyl)piperazine-1-ethanesulfonic acid (HEPES) were supplied by Macklin Biochemical Technology Co., Ltd. (Shanghai, China). ALP, ovalbumin (OVA), elastin (ELA), collagen (CA), thaumatin (THA), and pluronic F127 were obtained from Sigma-Aldrich (Shanghai, China). The other reagents were purchased from Guangzhou Chemical Reagent (Guangzhou, China). All the reagents were used as received without further purification. Ultrapure water (18.2 $\Omega.cm^{-1}$, purification by a Millipore system) was used throughout the experiments.

**Characterization.**

Powder X-ray diffraction (PXRD) patterns were carried out on a Bruker D8 Advance diffractometer (Cu Kα) at room temperature. $N_2$ adsorption isotherms were collected with a surface area and pore size analyzer (Micromeritics ASAP 2460). All the samples were pre-treated under 120 °C for 12 h before measurements. The morphology images were taken on a SU8010 ultra-high resolution field emission scanning electron microscope (SEM, Hitachi, Japan). To further investigate the Ce distribution in the MOFs, the samples were also observed using SEM integrated with an energy dispersive X-ray spectrometer (EDS, Oxford X-Max, UK). Transmission electron microscopy (TEM) characterization was performed using a JEM-2010HR microscope operating at 200 kV. The ultraviolet-visible (UV-vis) absorbance measurements were carried out on a 2800S spectrophotometer (SOPTOP, Shanghai), and the fluorescence spectra were recorded using an F97Pro spectrophotometer (Lengguang Technology, Shanghai) with a 150-W xenon. X-ray photoelectron spectroscopy (XPS) signals were analyzed by a Nexsa X-ray photoelectron spectrometer (Thermo Scientific, MA, USA). A confocal laser scanning microscope (CLSM 880 NLO, Carl Zeiss, Göttingen, Germany) was used to determine the distribution of dyes within MOFs. The Ce ratio within MOFs were measured with inductively coupled plasma mass (ICP-MS, Prodigy, Leeman, USA). The dynamic light scattering (DLS) and Zeta potentials of Ce-HMMOF were measured with a ZetaPALS analyzer (Brookhaven, USA).

**Preparation of Ce-UiO-66 and Ce-HMMOF.**

Synthesis of Ce-HMMOF: The synthetic procedures for Ce-HMMOF were based on the soft polymer template method.[1] Typically, 100 mg F127 powders were dispersed into 6 mL deionized water, followed by adding 0.3 mL HAc (5.1 mmol) and 500 mg $NaClO_4$ (3.5 mmol). This mixture was sonicated in order to get a homogenous dispersion. $(NH_4)_2Ce(NO_3)_6$ (548 mg, 1 mmol) and BDC (166 mg, 1 mmol) were added into above mixture. Then the mixed system was stirred for 20 min at 60 °C. The as-synthesized samples were centrifuged and washed with deionized water and DMF twice. To remove the template, the resultant solid was soaked in ethanol for two days at 60 °C, during which time the ethanol was exchanged with a fresh one every day. Finally, the product was dried at 60 °C in vacuum.

Synthesis of Ce-UiO-66: Ce-UiO-66 was synthesized according to the previous report with slight modifications.[2] 127.6 mg BDC was dissolved in 3.6 mL DMF, and then 0.2 mL formic acid and 1.2 mL $(NH_4)_2Ce(NO_3)_6$ (0.53 M) were added. The mixture was then stirred for 20 min at 100 °C. The as-synthesized samples were collected and washed with DMF twice to remove unreacted

reactants. To remove the DMF, the resultant solid was soaked in ethanol for two days at 60 °C, during which time the ethanol s exchanged with a fresh one. Finally, the product was dried at 60 °C in vacuum.

**Ce concentration measurement**

The Ce ratio of MOFs was evaluated by examining the content of Ce by ICP-MS. In a typical test, 2 mg Ce-HMMOF or Ce-UiO-66 was decomposed into 200 μL of heated nitric acid for 30 min and the solution was then diluted by 2% $HNO_3$ for ICP-MS detection. The Ce concentrations in the digested sample were quantified by a standard calibration curve (Figure S1). The Ce ratio in the MOFs could be converted from the measured Ce mass in the digested solution.

**Measurement of the ALP-like activity and the catalytic kinetic parameters.**

The ALP-mimic activities of Ce-UiO-66 and Ce-HMMOF were evaluated by tracing the fluorescence change of the reaction solution at 448 nm. In brief, 100 μL Ce-HMMOF (200 μg/mL) was added into the 800 μL NaOH solution (pH 10.0), followed by adding 100 μL of the prepared 4-MUP solution as a substrate. The dephosphorylation of 4-MUP could be evaluated based on the fluorescence emission wavelength at 448 nm (excitation at 365 nm) using a fluorescence spectrometer.

To determine the catalytic kinetic parameters, the dephosphorylation processes were performed as above described, and the used concentrations of 4-MUP ranged from 2.5 μM to 30 μM. The Michaelis-Menten model was fitted for the experimental values of the reaction rate and the substrate concentrations using the following equation:[3]

$$V_0 = \frac{V_{\max}[S]}{K_m + [S]} \quad (1)$$

Where $V_0$ and $V_{max}$ are the initial catalytic rate of nanozymes and the maximum rate of conversion, respectively. [S] is the substrate concentration of 4-MUP, and $K_m$ is the Michaelis-Menten constant. The catalyst rate constant ($k_{cat}$) is equal to the quotient of $V_{max}$ and the concentration of the nanozyme. The analysis was performed using the GraphPad Prism software (version 5.0.0, GraphPad Software, Inc., San Diego, CA).

**Dye penetration tests**

Dye penetration tests were carried out to explore the accessibility of binding sites for 4-MUP in the pore of UiO-66 and Ce-HMMOF. The as-synthesized UiO-66 and Ce-HMMOF particles (1mg) were suspended in 5 mL Rhodamine B (RhB) solution (10 μg/mL) at room temperature. After being incubated for 5 min, the samples were centrifuged and the precipitation was resuspended into 5 mL ethanol. Finally, RhB distribution within the particles was observed by CLSM.

**ATP and phosphorylated protein biosensing.**

The Ce-HMMOF based colorimetric biosensing was constructed for specific recognition of many larger biomolecules with phosphate esters, such as ATP and phosphorylated proteins. The reaction mixture contained 100 μL substrate, 800μL HEPES buffer (pH 8.5) and 100 μL Ce-HMMOF (2 mg/mL). The reactions were kept for 30 min at 37 °C and centrifuged, then 200 μL supernatant was added into 100 μL malachite solution, followed by adding 1% polyvinyl alcohol solution and 900 μL ultrapure water. The malachite solution was prepared by mixing ammonium molybdate (0.76 g), malachite green (0.036 g), sulfuric acid (3.2 g), and ultrapure water (7.4 mL).[4] After the color reaction for 20 min, the phosphate product was measured at 620 nm by UV-vis. All samples were performed in quadruplicate and standardized against a blank sample without a catalyst.

**Stability tests.**

The Ce-HMMOF and natural ALP with identical concentration were exposed to a series of harsh conditions. For thermal stability test, 3.75 μg/mL of Ce-HMMOF solution (ca. 1.5 μg/mL Ce) and 1.5 μg/mL of ALP solution were introduced into a preheated oven at temperatures from 40 to 80°C for 2 h. respectively. After cooling to room temperature, the retained activities after heating treatment were tested using 4-MUP as the substrate. For other tests, Ce-HMMOF and ALP were dispersed into trypsin (1 mg/mL), urea (6 M), and DMF solution, respectively, and both the concentrations of Ce-HMMOF (in terms of Ce) and ALP in each group were 1.5 μg/mL. After treating for 30 min, the retained activities were evaluated using 4-MUP as the substrate. In the stability tests, the original activity of Ce-HMMOF or ALP was set as 100%.

**Anti-interference experiment**

To investigate the probable interfering effects of co-existing substances on the detection of ATP, 5 mM KCl, 100 mM NaCl, 5 mM glucose (Glu), 25 mM methionine (Met), 250 mM glycine (Gly) or 150 mM proline (Pro) were introduced into ATP solution (100 μM), respectively. Then the Ce-HMMOF (2 mg/mL) was added to the mixture and cultured at 37 °C for 30 min. The contents of phosphate were measured as described previously. The competitive effect of co-existing substances on the detection of OVA was also assessed. The processes were similar to those for interfering studies of ATP determination, except that the concentration of OVA was 10 μM. To further evaluate the interfering effects of substances in real samples, the recovery experiments in 1% and 10% diluted human serum samples which were obtained from Third Affiliated Hospital of Guangzhou Medical University were performed.

## S2. Supplementary Figures

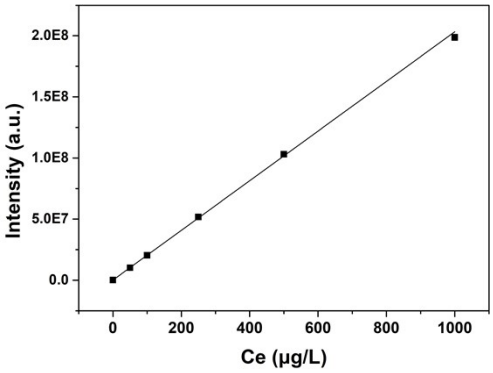


**Figure S1**. The calibration curve for Ce quantification using ICP-MS. The error bars are representative of the standard deviation of the triplicates.

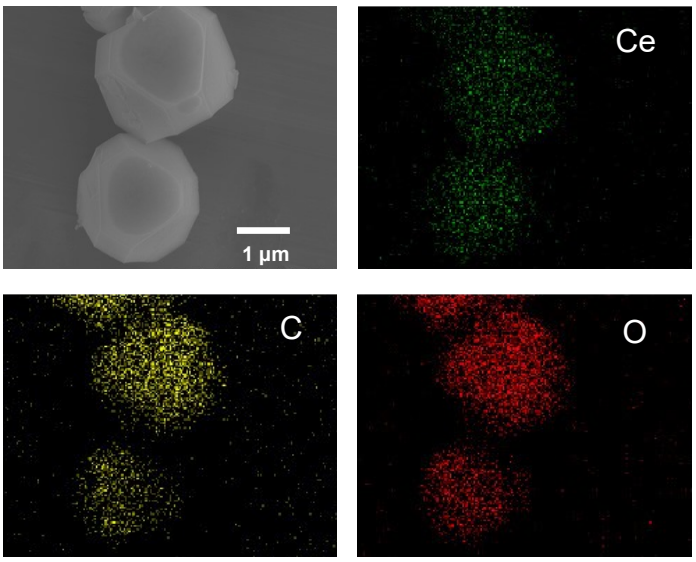


**Figure S2**. SEM image and the corresponding EDS elemental mapping of Ce, C, and O for Ce-HMMOF.

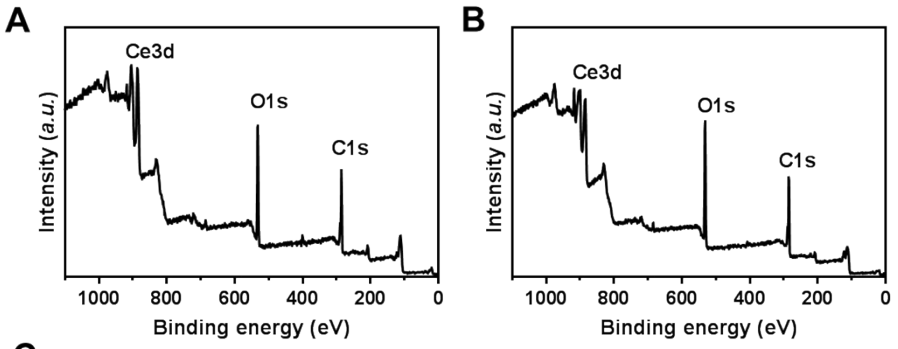


C

| | Ce (%) | $Ce^{4+}/Ce^{3+}$ | $Ce^{4+}$ (%) | $Ce^{3+}$ (%) |
|---|---|---|---|---|
| **Ce-UiO-66** | 6.17 | 1.755 | 63.71 | 36.29 |
| **Ce-HMMOF** | 6.23 | 1.994 | 66.05 | 33.96 |

**Figure S3**. XPS survey spectra of (A) Ce-UiO-66 and (B) Ce-HMMOF. (C) The valence states of cerium calculated according to the XPS spectrum.

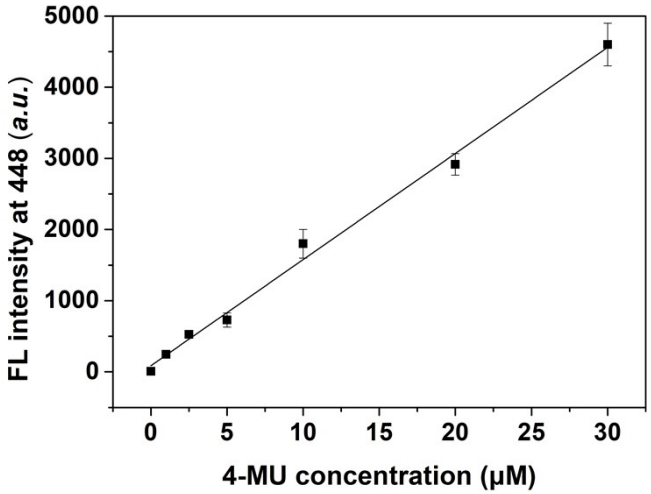


**Figure S4**. The calibration curve of 4-MU concentration in the enzymatic activity measurements for ALP, Ce-UiO-66 and Ce-HMMOF. The error bars are representative of the standard deviation of the triplicates.

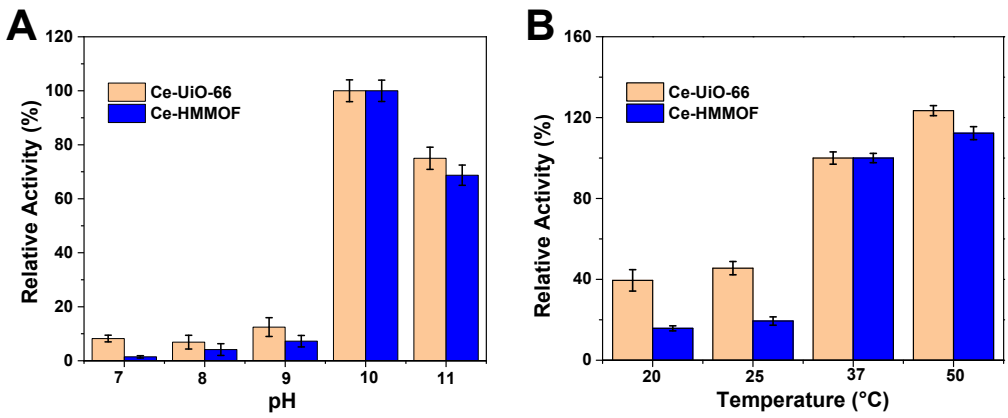


**Figure S5.** The effects of (A) pH and (B) temperature on 4-MUP hydrolysis over Ce-HMMOF.

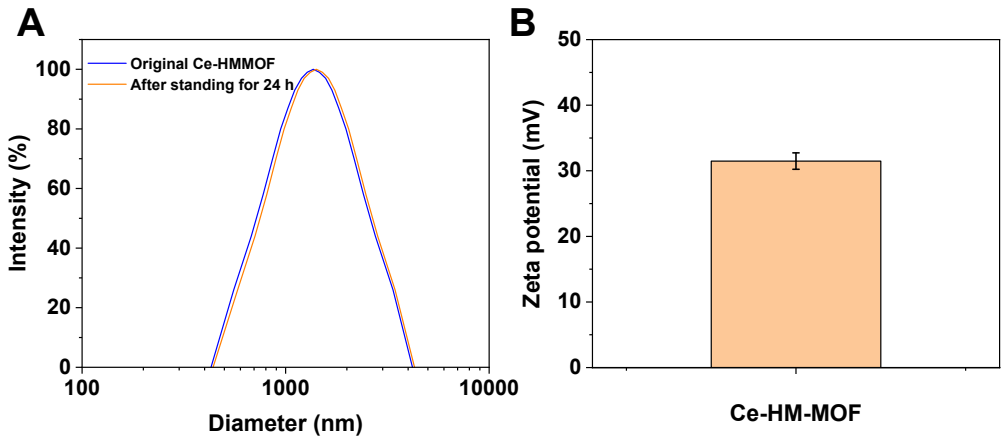


**Figure S6.** (A) The hydrodynamic particle size distribution of original Ce-HMMOF solution and the Ce-HMMOF after standing for 24h. (B) The zeta potential of Ce-HMMOF.

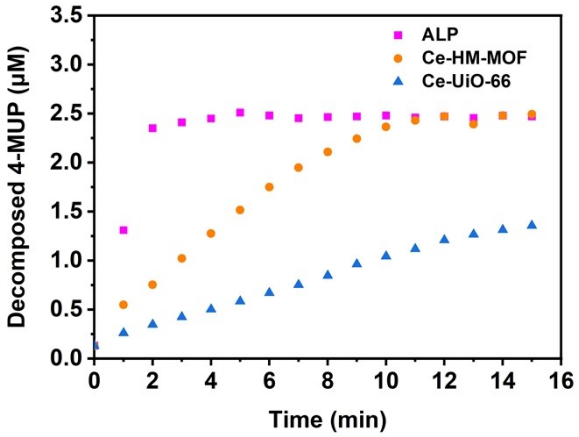


**Figure S7**. The catalytic kinetics curves of ALP, Ce-UiO-66 and Ce-HMMOF, respectively. Conditions: 2.5 μM 4-MUP. All the concentrations of ALP, Ce-UiO-66 (in terms of Ce) and Ce-HMMOF (in terms of Ce) were 5 μg/mL.

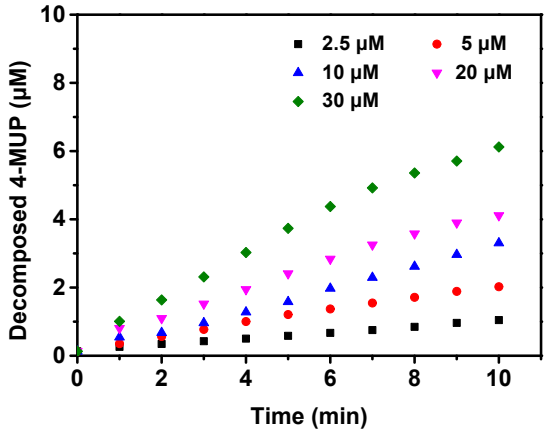


**Figure S8**. The concentration-dependent hydrolysis rate of 4-MUP in the catalytic process of Ce-UiO-66.

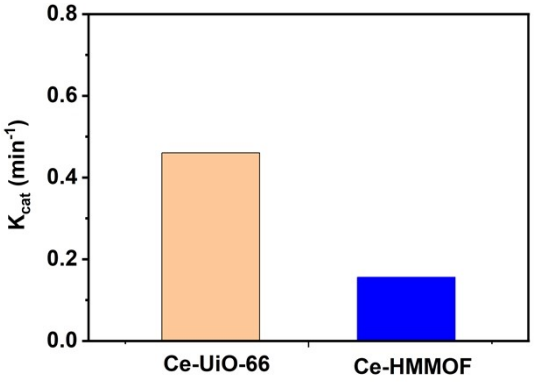


**Figure S9**. Comparison of the kinetic parameters of $K_{cat}$ between Ce-UiO-66 and Ce-HMMOF nanozymes.

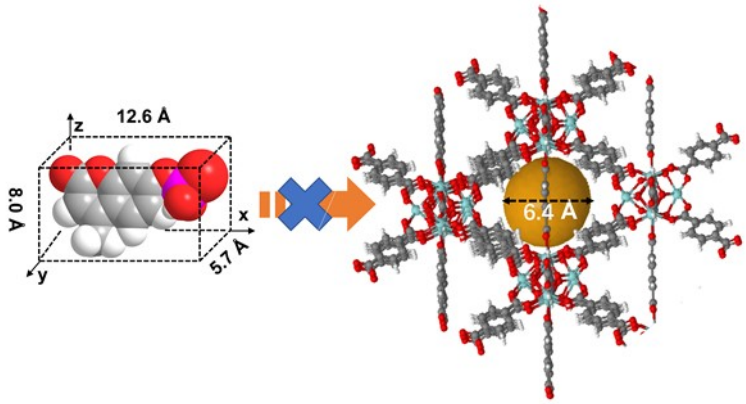


**Figure S10**. Structural illustration of the molecule size of 4-MUP and the crystallographic micropore of UiO-66.

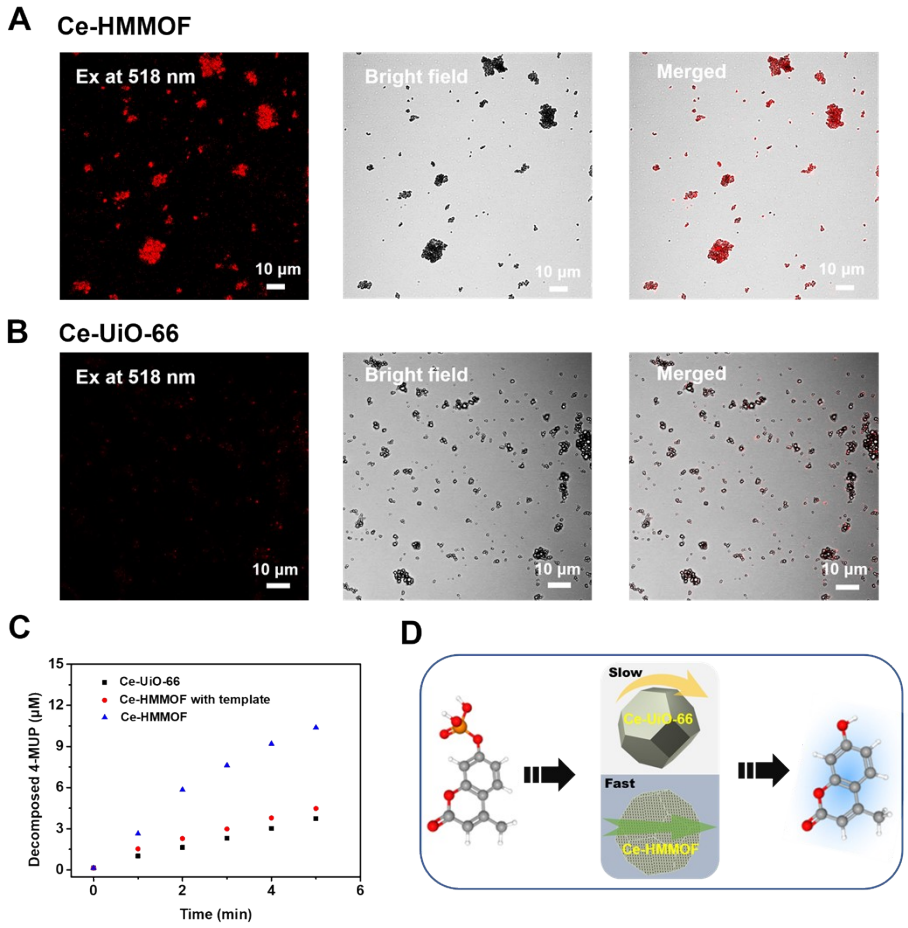


**Figure S11**. The CLSM images of (A) Ce-HMMOF and (B) Ce-UiO-66 after a fluorescent dye (RhB)-penetration experiment. (C) The catalytic kinetic curves of Ce-UiO-66, Ce-HMMOF and Ce-HMMOF with templates, respectively. Conditions: 30 μM 4-MUP. (D) Illustration of the key role of the mesochannels on the catalytic dephosphorylation of 4-MUP.

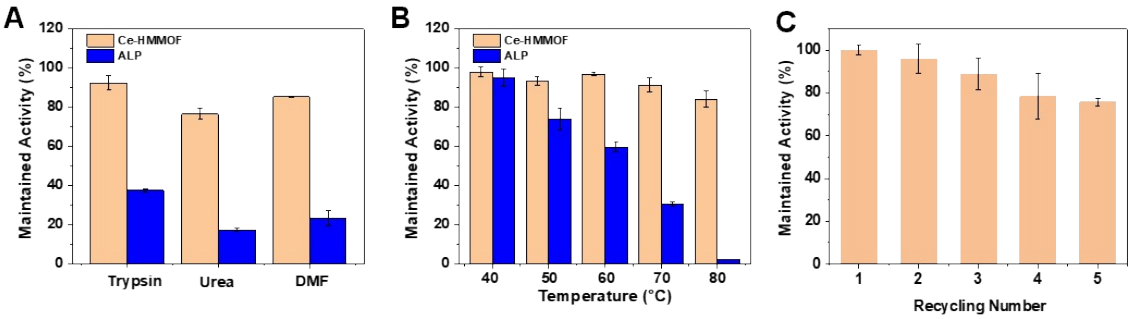


**Figure S12.** (A) The maintained bioactivity of Ce-HMMOF nanozyme and natural ALP after treatments with trypsin, urea, and DMF at 37 °C for 30 min, respectively. (B) The maintained bioactivity of Ce-HMMOF nanozyme and natural ALP after heating at 40-80 °C for 120 min. (C) The recyclability of Ce-HMMOF nanozyme for the catalytic dephosphorylation of 4-MUP. Both the mass concentrations of Ce-HMMOF (in terms of Ce) and ALP were 1.5 μg/mL, respectively.

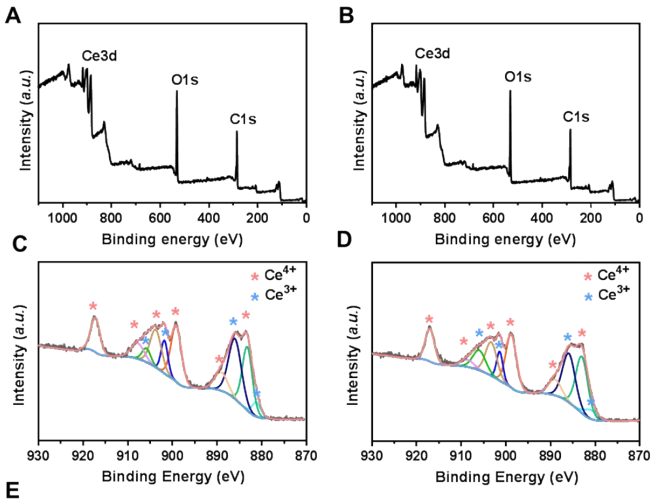


E

| | Ce (%) | $Ce^{4+}/Ce^{3+}$ | $Ce^{4+}$ (%) | $Ce^{3+}$ (%) |
|---|---|---|---|---|
| Original Ce-HMMOF | 6.23 | 1.944 | 66.05 | 33.96 |
| Ce-HMMOF after cycling test | 6.34 | 1.884 | 65.33 | 34.67 |

**Figure S13.** The XPS survey spectra (A) and high-resolution Ce3d spectra(C) of original Ce-HMMOF. The XPS survey spectra (B) and high-resolution Ce3d spectra (D) of Ce-HMMOF after recycling test. (E) The valence states of cerium calculated according to the XPS spectrum.

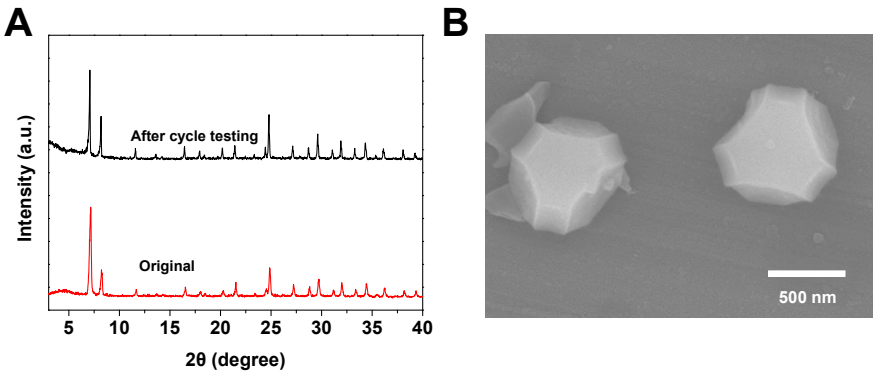


**Figure S14.** The (A) PXRD and (B) SEM images of Ce-HMMOF after cycle testing.

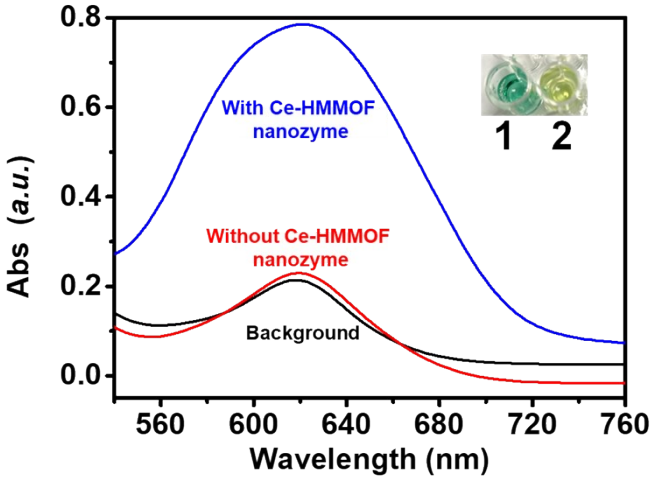


**Figure 15**. The UV-vis spectra of the biosensing assays with and without Ce-HMMOF nanozymes. The inset were the photographs of the signal output with Ce-HMMOF nanozymes (1) and without Ce-HMMOF nanozymes (2).

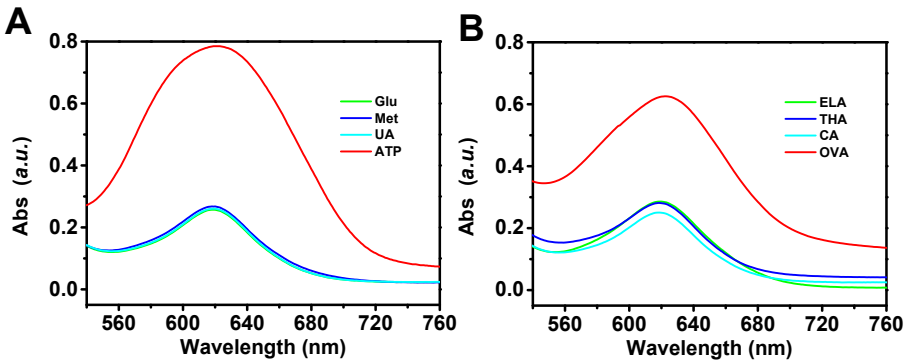


**Figure 16.** The selectivity for (A) ATP and (B) OVA by the Ce-HMMOF biosensing platform.

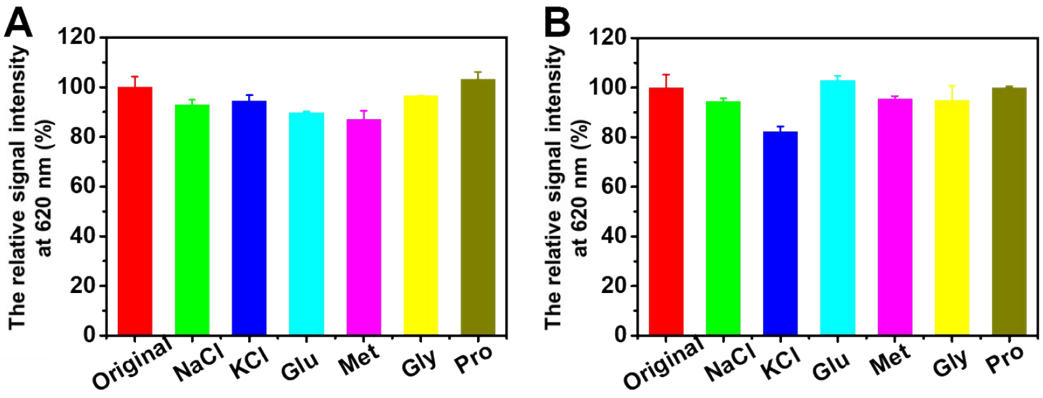


**Figure S17.** (A) The relative signal intensities for ATP biosensing when different interfering substances were co-existed with ATP. (B) The relative signal intensities for OVA biosensing when different interfering substances were co-existed with OVA. Glu: glucose; Met: methionine; Gly: glycine; Pro: proline.

## S3. Supplementary Tables

**Table S1.** Comparison of the linear range and the limit of quantitation (LOQ) of our Ce-HMMOF methods with other reported colorimetric methods for ATP biosensing.

| Methods | Linear range | LOQ | Reference |
|---|---|---|---|
| Gold nanoparticle | 4.4-132.7 μM | 4.4 μM | 5 |
| DNAzyme-aptamer | 6-1000 μM | 6 μM | 6 |
| Carbon dots | 0.05-2 mM | 0.05 μM | 7 |
| AuNPs with splited aptamer | 50-5000 μM | 50 μM | 8 |
| Organic molecules | 80-2200 μM | 80 μM | 9 |
| Ce-HMMOF | 0.5-100 μM | 0.5 μM | This work |

**Table S2.** The spiked recoveries of ATP and OVA in 1% human serum samples.

| Phosphorylated biomarkers | Samples | Target added (μM) | Target detected (μM) | Target Recovery (%) | RSD (n=3) (%) |
|---|---|---|---|---|---|
| ATP | 1 | 100 | 91.8 | 91.8 | 3.8 |
| | 2 | 10 | 10.6 | 106 | 3.4 |
| | 3 | 1 | 0.979 | 97.9 | 2.3 |
| OVA | 1 | 10 | 9.40 | 94.0 | 2.4 |
| | 2 | 1 | 0.93 | 93.7 | 4.6 |
| | 3 | 0.1 | 0.102 | 102 | 1.5 |

**Table S3**. The spiked recoveries of ATP and OVA in 10% human serum samples.

| Phosphorylated biomarkers | Samples | Target added (μM) | Target detected (μM) | Target Recovery (%) | RSD (n=3) (%) |
|---|---|---|---|---|---|
| ATP | 1 | 100 | 90.6 | 90.6 | 3.3 |
| | 2 | 10 | 10.3 | 103 | 3.7 |
| | 3 | 1 | 1.12 | 112 | 4.1 |
| OVA | 1 | 10 | 9.52 | 95.2 | 2.9 |
| | 2 | 1 | 1.09 | 109 | 4.3 |
| | 3 | 0.1 | 0.107 | 107 | 3.6 |

## S4. Supplementary References


1. K. Li, J. Yang, R. Huang, S. Lin and J. Gu, *Angew. Chem. Int. Ed.*, 2020, **59**, 14124-14128.
2. K. A. Lomachenko, J. Jacobsen, A. L. Bugaev, C. Atzori, F. Bonino, S. Bordiga, N. Stock and C. Lamberti, *J. Am. Chem. Soc.*, 2018, **140**, 17379-17383.
3. G. Chen, S. Huang, X. Kou, F. Zhu and G. Ouyang, *Angew. Chem. Int. Ed.*, 2020, **59**, 13947-13954.
4. K. Singh, A. Shukla, *Indian. J. Environ. Health*, 2003, **45**, 203-208.
5. J. Wang, L. Wang, X. Liu, Z. Liang, S. Song, W. Li, G. Li, C. Fan, *Adv. Mater.*, 2007, **19**, 3943-3946.
6. F. Liu, J. Zhang, R. Chen, L.Chen, L. Deng, *Chem. Biodivers.*, 2011, **8**, 311-316.
7. N. Huang, J. Wen, D. Yi, Z. Wei, Y. Long, H. Zheng, *Spectrochim. Acta. A*, 2022, **268**, 120658.
8. S. Cheng, B. Zheng, M. Wang, M. H. Lam, X. Ge, *Talanta*, 2013, **115**, 506-511.
9. F. Sancenón, A. B. Descalzo, R. Martínez-Máñez, M. A. Miranda, J. Soto, *Angew. Chem. Int. Ed.*, 2001, **40**, 2640-2643.